International Journal of Natural and Engineering Sciences 9 (2): 17-24, 2015
ISSN: 1307-1149, E-ISSN: 2146-0086, www.nobel.gen.tr

Battery and Solar Energy Conversion System for Solar Electric Vehicle using A Novel Hybrid Topology

Pezhman BAYAT[1*] Peyman BAYAT[1] S. M. Reza TOUSI[1] Alireza HATAMI[1]
[1] Department of Electrical Engineering, Faculty of Engineering, Bu-Ali Sina University, Hamedan, Iran

*Corresponding author:
E-mail: pezhman.bayat92@basu.ac.ir

Received: April 04, 2015
Accepted: May 12, 2015

Abstract

The large number of automobiles in use around the world has caused and continues to cause serious problems of environment and human life. Air pollution, global warming, and the rapid depletion of the earth's petroleum resources are now serious problems. For solving these problems, solar electric vehicles (SEVs) and hybrid electric vehicles (HEVs) have been typically proposed to replace conventional vehicles in the near future. They are high efficient, produces no local pollution, are silent, and can be used for power regulation by the grid operator. Up to now, SEVs and HEVs have been widely studied to improve vehicle performance. This paper for manage the energy between photovoltaic (PV) cells, battery and Brushless DC (BLDC) electric motor, proposed a novel topology for SEVs, where using bidirectional isolated DC-DC converter and boost DC-DC converter for the solar system and battery cells. For analyzing the effects of the proposed system, all of the components were simulated through MATLAB/SIMULINK environment.

Keyword: Converter, Electric Motor, Photovoltaic Cells, Solar Electric Vehicle (SEV).

INTRODUCTION

The use of renewable energy is increased due to continuous growth in energy consumption and the continuously decaying fossil fuels [1-2]. PV power has been a promising renewable energy source due to its zero pollution, ability to operate with much less restriction on location, and ease of maintenance [3]. The integration of PV power systems and energy storage schemes is one of the most significant issues in renewable power generation technology.

SEV is a vehicle that uses a combination of different energy sources to power an electric drive system, such as PV cells and batteries. In SEV the main energy source is assisted by one or more energy storage devices. Thereby the system cost, mass, and volume can be decreased, and a significant better performance can be obtained. However, SEVs still have critical issues which need to be solved.

Because the renewable systems in SEVs cannot provide a stable power for user, the renewable energy systems and battery can be utilized for the hybrid power systems. In the conventional PV system architecture, the PV power is transferred to the load through a unidirectional and a bidirectional converter where a considerable amount of power loss occurs in each conversion stage. Hence, the system efficiency deteriorates with the increasing number of power conversions. When the renewable energy systems cannot supply enough power for the load, the battery must replenish insufficient power. Whereas the whole power of the renewable energy systems cannot be used completely by the load, the surplus energy can be used to charge the battery.

When the battery pack is directly connected to a DC bus without a converter, efficiency of the system was reduced. Also, the battery life is degraded without proper control of charging and discharging of the battery. So distributed energy resources are not limited to PV and battery, which generate dc voltage. All of these resources have to be interfaced with a dc bus and feed power to the load; therefore, DC-DC power electronic converters are essential units [4, 5]. Because the bidirectional DC–DC converters can transfer the power between two DC sources in either direction, these converters are widely used for renewable energy hybrid power systems [6, 7, and 8]. Some cases of combining the solar array with the battery are investigated in [9]. The topologies of these converters have the isolated and non-isolated types for different applications. The isolated types include the flyback type [10, 11], forward-flyback type [12, 13], half-bridge type [14, 15] and full-bridge type [16, 17]. These converters can achieve large voltage gain by adjusting the turn's ratio of the transformer.

The bidirectional flyback converter has the advantages of simple structure and easy control. The appropriate solutions for large gain converters using a coupled inductor were presented in [18, 19]. A clamp circuit is proposed for recycling the leakage energy in a coupled inductor boost converter [18] or buck-boost converter [20]. The capacitor-diode clamp circuit acts in a similar way as the active clamp cell in a flyback converter, but it does not require an additional transistor. A similar idea is presented in [21], where the output voltage is obtained as the sum of the boost capacitor voltage and that of a voltage multiplier which serves as a rectifier inserted in the secondary winding circuit.

In this paper as shown in figure 1, for control of energy storage interface between PV cells, battery pack and BLDC electric motor, proposed a topology, which consist of a bidirectional isolated DC-DC converter and high step up DC-DC converter for the solar system and battery cells. The rest of this paper is organized as follows, PV cells, the battery, and proposed topology are modeled. Simulation results are presented and finally conclusion is given in last section.

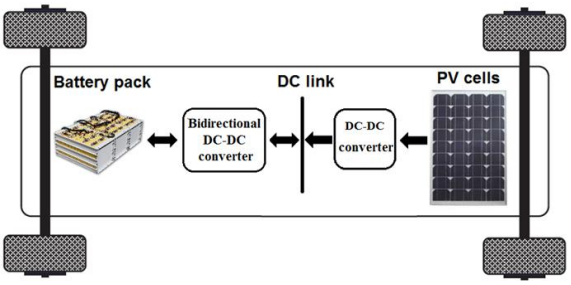

Figure 1. Energy exchange between PV cell, battery and DC link.

Photovoltaic Array Model

Figure 2 shows the equivalent circuit of the ideal photovoltaic cell. The basic equation from the theory of semiconductors [22] that mathematically describes the I-V characteristic of the ideal PV cell is:

$$I = I_L - I_0\left(e^{q(v+IR_s)/nKT} - 1\right) \quad (1)$$

The basic equation (1) of the elementary PV cell does not represent the I-V characteristic of a practical PV array. Practical arrays are composed of several connected PV cells and the observation of the characteristics at the terminals of the PV array requires the inclusion of additional parameters to the basic equations (2)-(8) [22]:

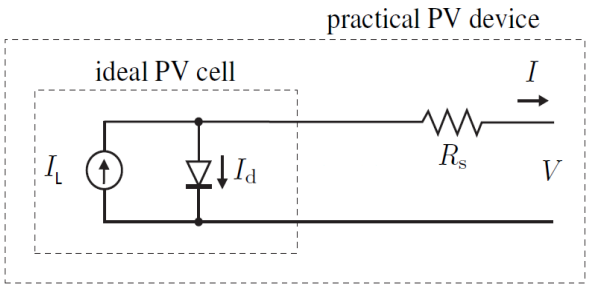

Figure 2. Single-diode model of the theoretical PV cell and equivalent circuit of a practical PV device including the series and parallel resistances.

Figure 3 shows the I-V curve originated from (1). The net cell current I is composed of the light-generated current I_L and the diode current I_d .

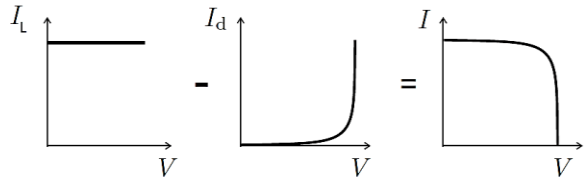

Figure 3. Characteristic I-V curve of the PV cell.

I-V characteristic of PV array is obtained by the following equations:

$$I_{L(T_1)} = G \times I_{SC(T_1,nom)} / G_{(nom)} \quad (2)$$

$$K_0 = \left(I_{SC(T_2)} - I_{SC(T_1)}\right) / \left(T_2 - T_1\right) \quad (3)$$

$$I_L = I_{L(T_1)}(1 + K_0(T - T_1)) \quad (4)$$

$$I_0 = I_{0(T_1)} \times (T / T_1)^{3/n} \times e^{-qV_0/nK \times (1/T - 1/T_1)} \quad (5)$$

$$I_{0(T_1)} = I_{SC(T_1)} / \left(e^{qV_{oc(T_1)}/nkT_1} - 1\right) \quad (6)$$

$$R_S = -\frac{dV}{dI_{V_{oc}}} - 1/X_V \quad (7)$$

$$X_V = I_{0(T_1)} \times q / nkT_1 \times e^{qV_{oc(T_1)}/nkT_1} \quad (8)$$

The following figure shows an example of a 24 volts and 54 watts photovoltaic arrays.

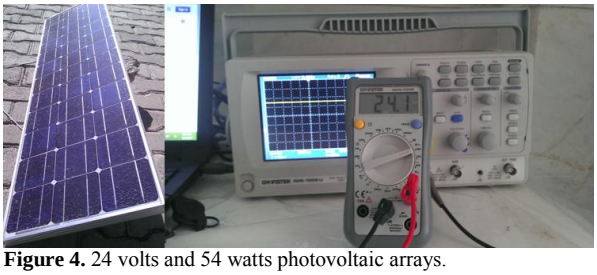

Figure 4. 24 volts and 54 watts photovoltaic arrays.

Battery Model

Lithium-ion batteries are now generally accepted as the optimal choice for energy storage in electric vehicles over lead-acid or nickel-metal-hydride batteries due to their superior power and energy densities [23]. The behavior of lithium-ion batteries depends strongly on different states of the battery like state of charge (SOC), temperature and current. The battery model used in this paper is based on a new high-power lithium ion cell [24], which shows high power density and high efficiency.

Control Voltage Level

A small size of PV system; starts up from a few hundred watts to a few kilowatts, is more and more adopted in households due to attention of global warming and energy conservation. However, output power of PV array is directly affected by two uncontrollable parameters, i.e. sun radiation or irradiance (W/M^2) and ambient temperature (C°) [25]. Consequently, output power of PV array has widely variations. In order to obtaining full utilization of PV system, a high efficiency converter operated is a need [26].

PV systems consist of a solar panels, DC-DC voltage converters, controllers and batteries. DC-DC voltage converters are used for matching the characteristics of the load with that of the solar panels [27]. DC-DC voltage converters are classified into three categories boost converters, buck converters and buck-boost converters.

As shown as in figure 1, for control voltage level between solar cell, battery and DC link, high step up DC-DC converter for photovoltaic system and bidirectional isolated DC–DC converter for battery cells are used.

Bidirectional isolated DC–DC converter for battery application

In the bidirectional dc-dc converters, isolation is normally provided by a transformer [28]. One kind of isolated bidirectional dc-dc converter is based on the half-bridge in the primary side and on the current fed push-pull in the secondary of a high frequency isolation transformer [29]. The converter operation is described for both modes; in the presence of dc bus the battery is being charged, and in the absence of the dc bus the battery supplies power. [30, 31]. A novel hybrid bidirectional dc–dc converter was derived and presented in [32]. In this paper, characteristics

of the proposed converter in [32] will be analyzed in MATLAB/SIMULINK environment and used in proposed energy storage Interface.

As seen through figure 5, the boost type half bridge high frequency inverter with the switches operating by 50% duty cycle is in the primary side of the transformer. S3 and S4 are controlled by duty-cycle, d, to change the operating modes, when input voltage is variable in the wide range. Two transformers, T1 and T2, with the paralleled primary windings and series-wound secondary windings are utilized to realize isolation and boost the low input voltage. Voltage double circuit in secondary side of the transformer is to get higher voltage conversion ratio. The leakage inductances of the transformers are the interface and energy transfer elements between the two high frequency inverters. According to different power flow directions, operational modes of the presented converter can be divided into two modes, Boost mode and Buck mode. In Boost mode, the power is delivered from the PV cells to the high voltage DC bus, which means energy is from low voltage side to the high voltage side.

In order to verify the operation principle of the presented converter, performance of the system is studied through simulation in MATLAB/SIMULINK.

The following figures show switching for this bidirectional isolated DC–DC converter:

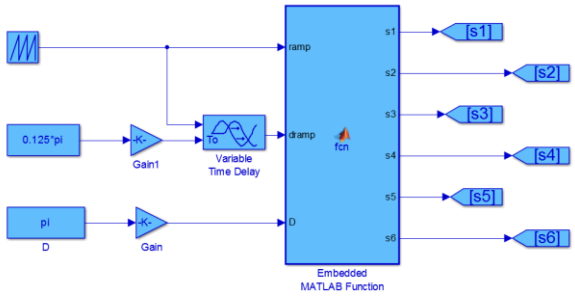

Figure 6. Switching for bidirectional isolated DC–DC converter.

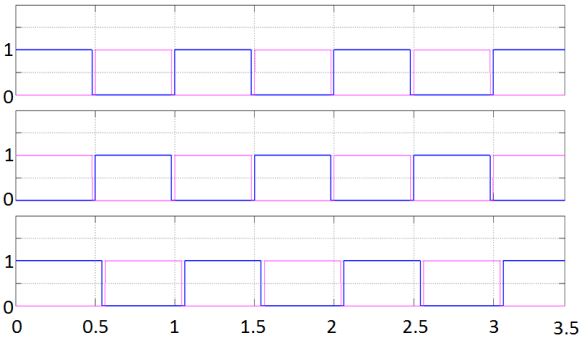

Figure 7. The first pulse corresponding to S1, S2, second pulse corresponds to S3, S4, and the third pulse corresponds to S5, S6.

Figure 8, shows simulation waveforms in $V_{batt} = 30V_{DC}$ (input power 750 W) and d = π and figure 9, shows simulation waveforms in $V_{batt} = 30V_{DC}$ (input power 750 W) and d = 0.65π.

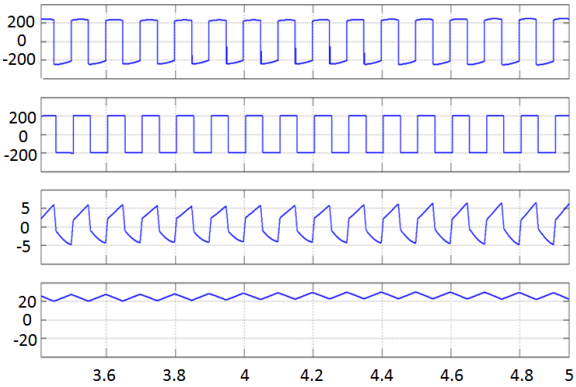

Figure 8. $V_{T1}+V_{T2}$ (First waveform), V_{co} (second waveform), i_{L2} (third waveform), i_{L1} (fourth waveform).

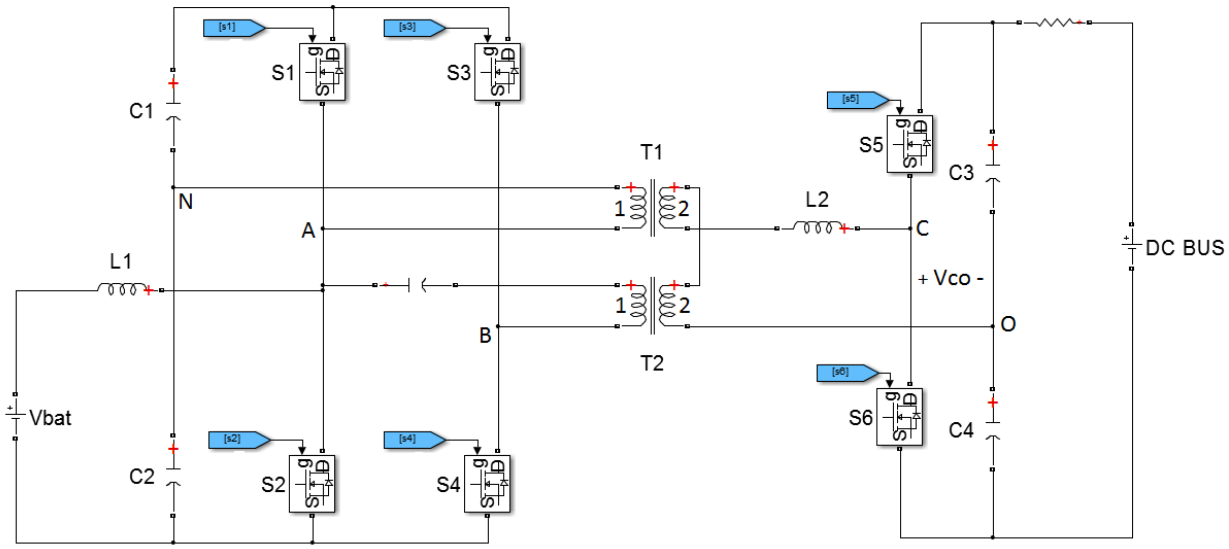

Figure 5. Bidirectional isolated DC–DC converter for battery application.

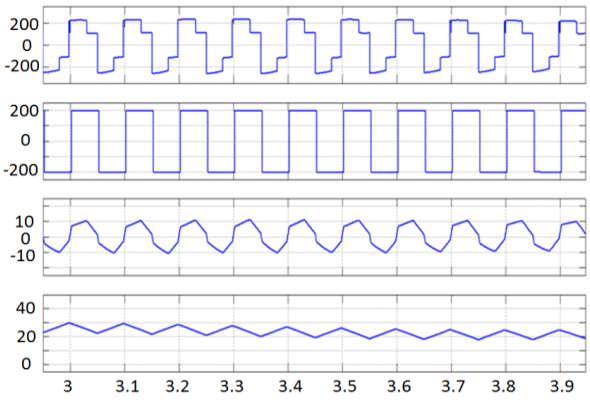

Figure 9. $V_{T1}+V_{T2}$ (First waveform), V_{co} (second waveform), i_{L2} (third waveform), i_{L1} (fourth waveform).

Figure 10 shows the voltage and current for other areas of the converter in $V_{batt}=30V_{DC}$ (input power 750 W) and d = 0.65π.

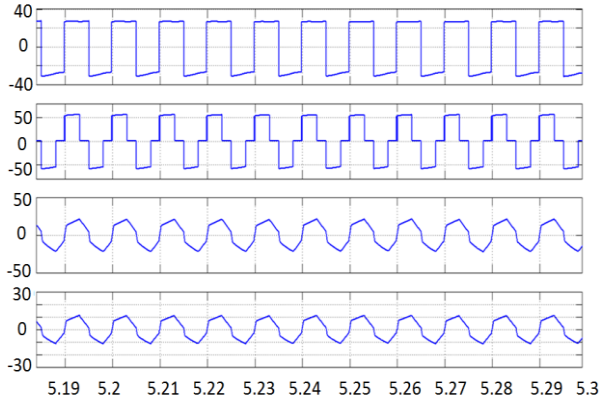

Figure 10. V_{AN})First waveform), V_{AB} (Second waveform), i_{T1} (third waveform), i_{T2} (fourth waveform).

In figure 11, the gate drive signals and the drain–source voltages of switches S2, S4, and S6 are presented, respectively. These waveforms demonstrate that the voltage across switches has decreased to zero before the gate drive signal is given, which verifies the turn on ZVS operation.

This converter is well suited for battery charging and discharging circuits. The battery model has to satisfy different requirements due to the applications, for example it has to be able to deal with very fast changing as well as quite static input signals.

High step up DC-DC converter for photovoltaic system

Very high step-up voltage transfer gains are required by many modern applications such as high-intensity discharge ballasts for automobile headlamps, fuel-cell and solar-cell energy conversion systems, and so on.

The basic DC-DC converters can attain a high voltage transfer gain but practically the large step-up voltage ratio is limited due to limitation by the extremely high duty ratio. The requirements also include good efficiency, little electromagnetic interference noise, operation at high switching frequency, and a small count of elements. Many non-isolated topologies have been presented to obtain high step-up voltage gain in the past decade [33, 34]. These non-isolated converters can be used with the coupled inductor technique [35], cascaded technique [36, 37], and switched-inductor and switched-capacitor techniques [38] to obtain high voltage gain with the appropriate duty ratio.

However, non-isolated converters cannot meet the safety standards needed in galvanic isolation. In order to meet the safety standards of galvanic isolation, some isolated converters for high-step-up applications have been proposed. These converters are secondary-series boost converters [39, 40], voltage-lift techniques [41, 42], and boost-type converters integrated with a transformer [43, 44] to obtain high voltage gain.

In proposed method for manage energy between solar cells and DC bus, high step-up DC–DC converter with coupled-inductor and voltage doubler circuits which proposed in [45] is used. Figure 12 shows the circuit configuration of this converter, which consists of two active switches S1 and S2, one coupled inductor, four diodes D1−D4, and two output capacitors C1 and C2. The coupled inductor is modeled as a magnetizing inductor Lm, a primary leakage inductor Lk1, a secondary leakage inductor Lk2, and an ideal transformer. Capacitors CS1 and CS2 are the parasitic capacitors of S1 and S2, respectively.

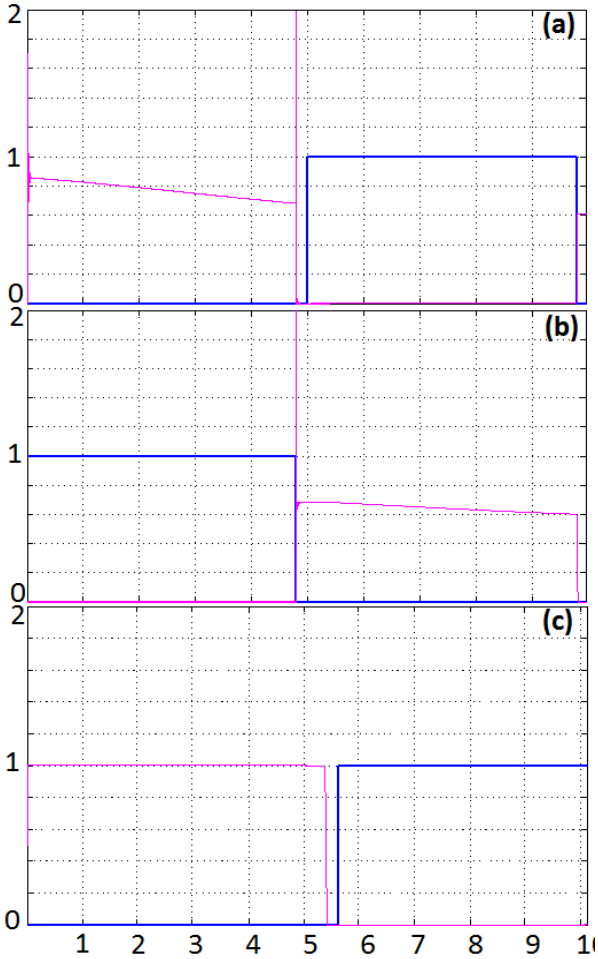

Figure 11. Drain source voltage v_{ds} and gate drive signal v_{gs} of the switches in V_{batt} = 30 V_{DC} and input power 750 W.
(a) S_2: v_{gs2} (blue waveform), and v_{ds2} (Purple waveform)
(b) S_4: v_{gs4} (blue waveform) and v_{ds4} (Purple waveform)
(c) S_6: v_{gs6} (blue waveform) and v_{ds6} (Purple waveform)

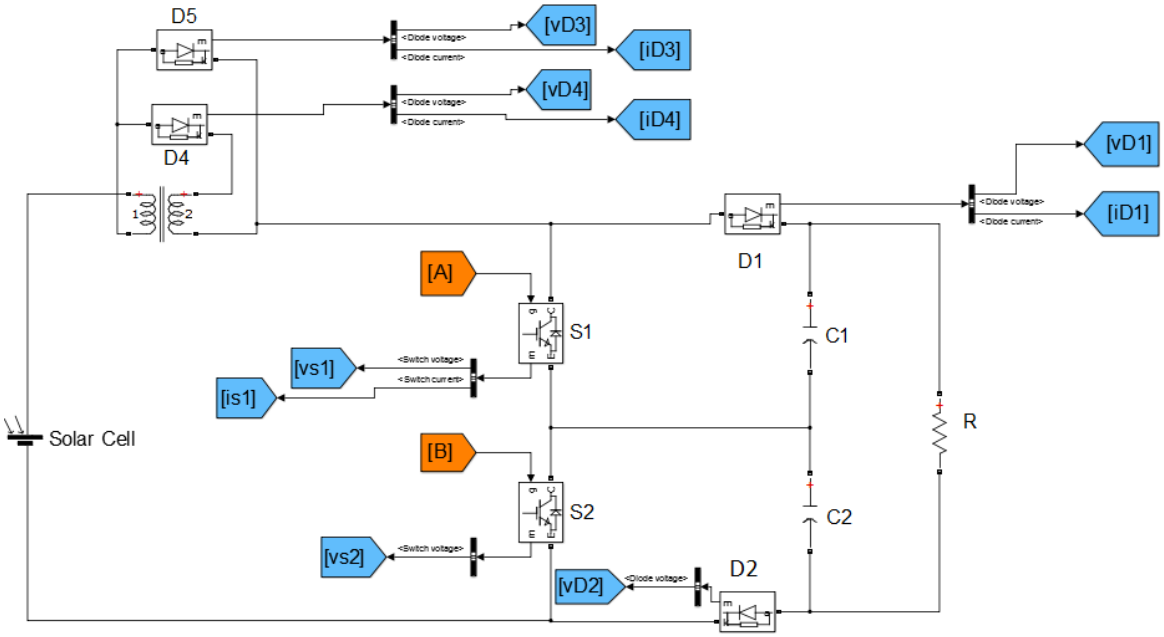

Figure 12. High step-up DC–DC converter with coupled-inductor and voltage doubler circuits.

The following figure shows switching for high step-up DC–DC converter:

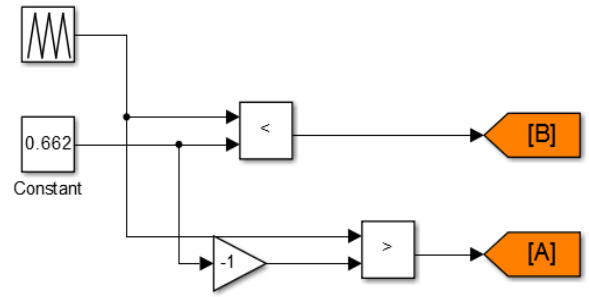

Figure 13. Switching for high step-up DC–DC converter.

Under the operating conditions V_{in}= *24* V, V_o= *204* V, and P_o= *250* W, some simulation waveforms are shown in Figures 14–18. Figures 14, 15 and 16 show some simulation voltage waveforms. It is seen that V_{s1}, V_{s2}, V_{D1}, and V_{D2} are equal to half of the output voltage during the steady-state period. However, the ringing phenomenon of V_{s1} and V_{s2} is caused by the line inductors and parasitic capacitors of S_1 and S_2 when S_1 and S_2 are turned off. Thus, the ringing phenomenon must be taken into consideration for choosing S_1 and S_2. Figure 17 shows some simulation current waveforms, which agree with the operating principle and the steady-state analysis. However, the ringing phenomenon exists in i_{D4}. One must consider this phenomenon for choosing D_4. As shown in Figure 18, the voltages across C_1 and C_2 are equal, and they are also equal to half of the output voltage.

Figure 19 shows the DC link voltage which obtained by battery and solar cells in different radiation, sunlight intensity in terms of watts per square meter, output voltage of battery cells and output voltage of PV arrays.

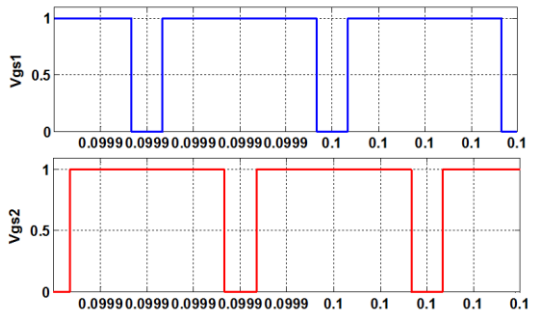

Figure 14. Simulation waveforms of V_{gs1} and V_{gs2}.

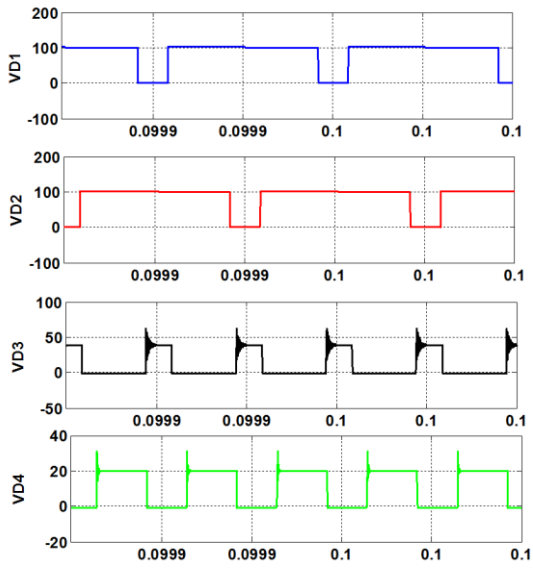

Figure 15. Simulation waveforms of V_{D1}, V_{D2}, V_{D3} and V_{D4}.

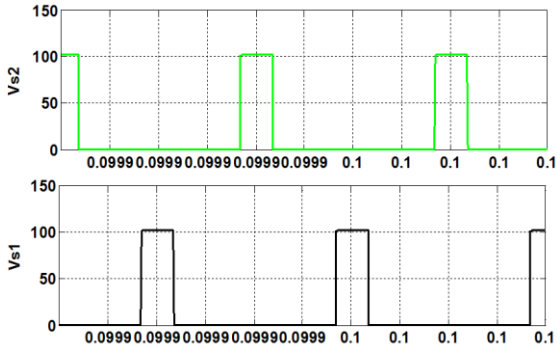

Figure 16. Simulation waveforms of V_{S2} and V_{S1}.

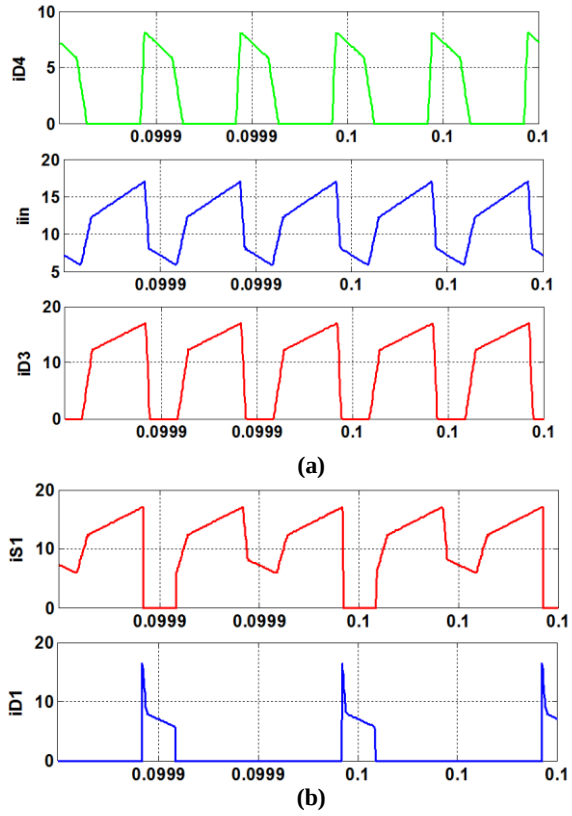

Figure 17. Simulation waveforms. (a) I_{D4}, I_{in} and I_{D3}. (b) I_{S1} and I_{D1}.

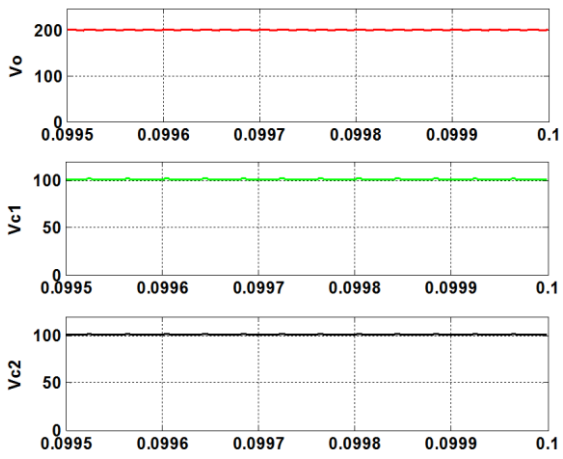

Figure 18. Simulation waveforms for V_O, V_{C1} and V_{C2}.

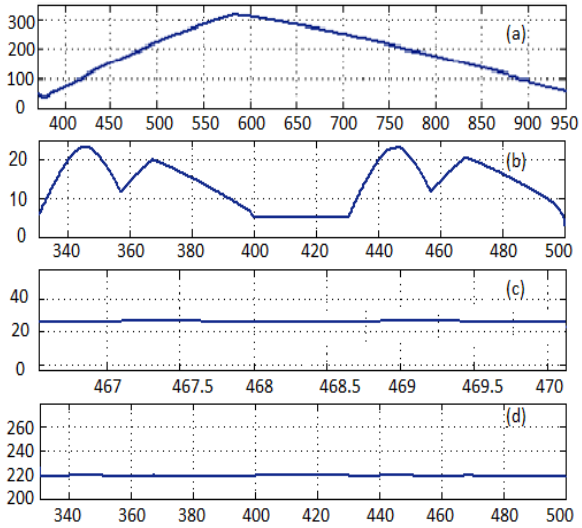

Figure 19. (a) Sunlight intensity in terms of watts per square meter
(b) Output voltage of PV arrays in different radiations
(c) Voltage of battery cells
(d) DC bus voltage

CONCLUSION

The power generation systems using low-DC renewable energy sources such as photovoltaic module and fuel cell need a high step-up DC-DC converter to interface the low-DC voltage to the high DC voltage distribution network. It is well known that the output voltage of PV arrays fluctuates with the output current and climate conditions such as solar radiation and ambient temperature. In other words, the output voltage of PV arrays has a wide variation range. It is thus imperative for the front-end dc/dc converter to achieve a high efficiency over the entire input-voltage range. Because the bidirectional DC–DC converters can transfer the power between two DC sources in either direction, these converters are widely used for renewable energy hybrid power systems, so this paper for control of energy storage interface between PV cell, battery and DC bus, proposed a novel topology. Different parts of this topology are discussed, eventually various voltages and currents converters simulated in MATLAB/SIMULINK environment.

NOMENCLATURE

I_0	Saturation current for diode [A]
q	Electronic charging [1.6e-19 C]
n	Quality factor of diode
K	Boltzman's constant [1.38e-23 J k^{-1}]
T	Temperature [℃]
T_1	Reference temperature-1 [℃]
T_2	Reference temperature-2 [℃]
G	Irradiance [w / m^2]
I_{sc}	Short circuit current [A]
V_{oc}	Open circuit voltage [V]
V_g	Gap voltage band [V]

REFERENCES

[1] Ansari M. F., Chatterji S. and Iqbal A., 2010. A fuzzy logic control scheme for a solar photovoltaic system for a maximum power point tracker, Int. J Sustainable Energy, 29(4): 245-255.

[2] Brunton S., Rowley C., Kulkarni S., and Clarkson C., 2010. Maximum power point tracking for photovoltaic optimization using ripple-based extremum seeking control, IEEE Trans. Power Electron., 25(10): 2531-2540.

[3] Abhilash Ch., Shirisha R., Khaja R., 2013. Analysis of Full Bridge Boost Converter for Wide Input Voltage Range, International Journal of Engineering and Computer Science, 2(8): 2397-2402.

[4] Kramer W., Chakraborty S., Kroposki B. and Thomas H., 2008. Advanced power electronic interfaces for distributed energy systems—I: System and topologies, National Renewable Energy Laboratory, Golden, CO, Tech. Rep. NREL/TP-581–42672.

[5] Seo G. S., Baek J., Choi K., Bae H. and Cho B., 2011. Modeling and analysis of DC distribution systems, in Proc. IEEE 8th Int. Conf. Power Electron. ECCE Asia, 223–227.

[6] Venkatesan K., 1989. Current mode controlled bidirectional flyback converter. Proc. IEEE PESC, 835–842.

[7] Huber L., Jovanovic M. M., 1999. Forward-flyback converter with current-doubler rectifier: analysis, design, and evaluation results, IEEE Trans. Power Electron., 184-192.

[8] Li H., Peng F. Z., Lawler J. S., 2003. A natural ZVS medium-power bidirectional DC–DC converter with minimum number of devices, IEEE Trans. Ind. Appl., 525-535.

[9] Vishwas K, Suryanarayana K, Renukapp N.M. and Prabhu L.V., 2014. Modeling of Multiphase Boost Converter for Solar Battery Charging System, IEEE Students Conference on Electrical, Electronics and Computer Science, Bhopal, 1-6.

[10] Venkatesan, K., 1989. Current mode controlled bidirectional flyback converter, Proc. IEEE PESC, 835-842.

[11] Chen G., Lee Y. S., Hui S.Y.R., Xu D. and Wang Y., 2000. Actively clamped bidirectional flyback converter, IEEE Trans. Ind. Electron., 47(4): 770-779.

[12] Huber L. and Jovanovic M.M., 1999. Forward-flyback converter with current-doubler rectifier: analysis, design, and evaluation results, IEEE Trans. Power Electron., 14(1): 184-192.

[13] Zhang F. and Yan Y., 2009. Novel forward–flyback hybrid bidirectional DC–DC converter', IEEE Trans. Ind. Electron., 56(5): 1578-1584.

[14] Li H., Peng F.Z. and Lawler, J. S., 2003. A natural ZVS medium-power bidirectional DC–DC converter with minimum number of devices, IEEE Trans. Ind. Appl., 2003, 39(2): 525-535.

[15] Lin B.R., Huang C.L. and Lee Y.E., 2008. Asymmetrical pulse-width modulation bidirectional DC–DC converter', IET Power Electron., 1(3): 336-347.

[16] Mi C., Bai H., Wang C. and Gargies S., 2008. Operation, design and control of dual H-bridge-based isolated bidirectional DC–DC converter, IET Power Electron., 1(4): 507-517.

[17] Naayagi R.T., Forsyth, A.J. and Shuttleworth R., 2012. High-power bidirectional DC–DC converter for aerospace applications, IEEE Trans. Power Electron., 2012, 27(11): 4366-4379.

[18] Zhao Q., Tao F. and Lee F.E., 2001. A front-end DC/DC converter for network server applications, in Proc. IEEE PESC, 1535-1539.

[19] Wu H.T.F., Lai Y.S., Hung l.e. and Chen Y.M. 2008. Boost converter with coupled inductors and buck-boost type of active clamp, IEEE Trans. ind. Electron, 55(1): 154-162.

[20] Zhao Q. and Lee F.E., 2003. High-efficiency, high step-up DC-DC converters, IEEE Trans. Power Electron., 18(1): 65-73.

[21] Baek W., Ryoo M.H., Kim T. J., Yoo D. W. and Kim 1.S., 2005. High boost converter using voltage multiplier, in Proc. Ann. Cotif. iEEE ind. Electron. Soc. (iECON'05), 567-572.

[22] Walker G.R., 2001. Evaluating MPPT Converter Topologies Using A MATLAB PV Model" Journal of Electrical & Electronics Engineering. Australia. 21(1): 49-56.

[23] Burke A., 2007. Batteries and ultracapacitors for electric, hybrid, and fuel cell vehicles, Proc. IEEE, 95(4): 806-820.

[24] A123 Systems. [Online]. Available: http://www.a123systems.com.

[25] Gonzalez L.F., 2006. Model of Photovoltaic Module in MATLAB, iiC1BELEC '06.

[26] Hardik P.D. and Patel H.K., 2007, Maximum Power Point Algorithm in PV Generation: An Overview, in Proc. IEEE PEDS'07, 624-630.

[27] Tasi-Fu W. and Yu-Kai C., 1998. Modeling PWM DC/DC Converters out of Basic Converter Units, IEEE Trans Power Electron, 13(5): 870-881.

[28] Lai J.S. and Nelson D.J., 2007. Energy management power converters in hybrid electric and fuel cell vehicles, in Proc. IEEE Ind. Electron., Taipei, Taiwan, 95(4): 766-777.

[29] Jain M., Jain P.K. and M. Daniele, 1997. Analysis of a bi-directional dc-dc converter topology for low power application, in Conf. Rec. of IEEE 1997 Canadian Conference on Electrical and Computer Engineering, St. John's, NF, 2: 548-551.

[30] Santhi M., Rajaram R. and Raj I.G.C., 2006. A ZVCS lc-resonant push-pull power converter circuit for battery-fuel cell hybrid systems," in Conf. Rec. of IEEE Conference on Electric and Hybrid Vehicles, Pune, India, 1-6.

[31] Doncker R.W., Divan D.M. and Kheraluwala M.H., 1991. A three-phase softswitched high power density dc-to-dc converter for high power applications, IEEE Tran. Ind. Appl., 27(1): 63-73.

[32] Zhang Z., Ouyang Z., Thomsen O.C. and Andersen M.A.E., 2012. Analysis and Design of a Bidirectional Isolated DC–DC Converter for Fuel Cells and Supercapacitors Hybrid System" IEEE Transactions on Power Electronics, 27(2): 848-859.

[33] Wu T.F., Lai Y.S., Hung J.C. and Chen Y.M., 2008. Boost converter with coupled inductors and buck–boost type of active clamp, IEEE Trans. Ind. Electron., 55(1): 154-162.

[34] Luo F.L. and Ye H., Positive output multiple-lift push–pull switched capacitor Luo-converter, IEEE Trans. Ind. Electron., 51(3): 594-602.

[35] Yang L.S., Liang T.J., Lee H.C. and Chen J.F., 2011. Novel high step up dc–dc converter with coupled-inductor and voltage-doubler circuits," IEEE Trans. Ind. Electron., 58(9): 4196-4206.

[36] Tseng K.C. and Liang T.J., 2004. Novel high-efficiency step-up converter, Proc. Inst. Elect. Eng. Elect. Power Appl., 151(2): 182-190.

[37] Chen S.M., Liang T.J., Yang L.S. and Chen J.F., 2011. A cascaded high step-up dc–dc converter with single switch for micro source applications, IEEE Trans. Power Electron., 26(4): 1146-1153.

[38] Axelrod B., Berkovich Y. and Ioinovici A., 2006. Switched coupled-inductor cell for dc–dc converters with very large conversion ratio, in Proc. IEEE IECON, 2366-2371.

[39] Li W., Liu J., Wu J. and He X., 2007. Design and analysis of isolated ZVT boost converters for high-efficiency and high-step-up applications, IEEE Trans. Power Electron, 22(6): 2363-2374.

[40] Zhao Y., Li W., Deng Y. and He X., 2010. Analysis, design, and experimentation of an isolated ZVT boost converter with coupled inductors, IEEE Trans. Power Electron, 26(2): 541-550.

[41] Kuo P.H., Liang T.J., Tseng K.C., Chen J.F. and Chen S.M., 2010. An isolated high step-up forward/flyback active-clamp converter with output voltage lift, in Proc. IEEE ECCE, 542-548.

[42] Lin B.R., Liang Y.S., Tung C.Y., Chen J.J. and Shien J.J., 2009. Activeclamp ZVS converter with step up voltage conversion ratio, in Proc. IEEE ICIEA, 2032-2037.

[43] Chung S.K., Lim J.G. and Song Y., 2010. Active clamped three-phase isolated boost converter with series output connection for high step-up applications, in Proc. IEEE ECCE, 1090-1097.

[44] Oliveira S.V.G. and Barbi I., 2011. A three-phase step-up dc–dc converter with a three-phase high-frequency transformer for dc renewable power source applications, IEEE Trans. Ind. Electron., 58(8): 3567-3579.

[45] Yang L.S., Liang T.J., Lee H.c. and Chen J.F., 2011. Novel High Step-Up DC–DC Converter with Coupled-Inductor and Voltage-Doubler Circuits, in Industrial Electronics, IEEE Transactions, 58(9): 4196-4206.